

INVESTIGATION OF TUNED LIQUID DAMPERS UNDER LARGE AMPLITUDE EXCITATION

By Dorothy Reed,¹ Member, ASCE, Jinkyu Yu,² Harry Yeh,³ Member, ASCE, and Sigurdur Gardarsson⁴

ABSTRACT: The behavior of tuned liquid dampers (TLD) was investigated through laboratory experiments and numerical modeling. Large amplitude excitation is the primary focus, as previous research was limited to small amplitude motion. Time histories of the base shear force and water-surface variations were measured by precisely controlled shaking table tests. The results are compared with a numerical model. The random-choice numerical method was used to solve the fully nonlinear shallow-water wave equations. The results suggest that the model captures the underlying physical phenomenon adequately, including wave breaking, for most of the frequency range of interest and over a wide range of amplitude excitation. It was found that the response frequency of tuned liquid dampers increases as excitation amplitude increases, and the TLD behaves as a hardening spring system. To achieve the most robust system, the design frequency for the damper, if it is computed by the linearized water-wave theory, should be set at the value lower than that of the structure response frequency; hence, the actual nonlinear frequency of the damper matches the structural response. It was found that, even if the damper frequency had been mistuned slightly, the TLD always performed favorably; we observed no adverse effect in the wide range of experimental parameters tested in this study.

INTRODUCTION

In recent years, the construction of lightly damped, flexible tall buildings in regions of seismic and extreme-wind risk has created concern in the structural engineering community. In recognition of the serviceability issues, engineers have created artificial damping devices. Of these devices, tuned liquid dampers (TLDs) have proven a successful passive vibration mitigation system (Kareem and Sun 1987; Tamura et al. 1988; Fujii et al. 1990; Wakahara et al. 1992; Fediw et al. 1993; Wakahara 1993). However, these systems have not been thoroughly investigated and are often designed using simplistic methods. This limitation greatly restricts the designer's ability to effectively employ the TLD as a damping device.

The major objective of the present study is to analyze the behavior of TLDs through both experimental investigation and numerical modeling. In particular, the performance of these damping devices under large amplitude excitation is important, because previous studies were limited to small amplitude excitation. Although gaining an understanding of the behavior of the liquid in the tank itself was considered paramount, the role of the liquid in dissipating energy is explicitly investigated. In this paper, the results of an experimental investigation of TLDs under shaking table excitation for an expanded range of frequencies and amplitudes, coupled with a new numerical modeling of the liquid behavior in the tank, are presented.

The classical modeling of the single degree of freedom (SDOF) structural system damped by a TLD is given as follows with reference to Fig. 1:

$$\ddot{x}_s(t) + 2\zeta_s\omega_s\dot{x}_s(t) + \omega_s^2x_s(t) = F_e + F_b \quad (1)$$

where x_s = displacement of the structural system; ζ_s = coefficient of damping of the structure; ω_s = structural natural frequency in radians/second; F_e = excitation force; and F_b = force, usually referred to as the base shear, provided by the

TLD along the same axis as the excitation. The base shear force is ideally modeled as the hydrodynamic force F_b induced by the liquid sloshing as given in the following equation with reference to Fig. 2:

$$F_b \approx \frac{1}{2} \rho g b [h_l^2 - h_r^2] \quad (2)$$

where ρ = density, g = gravity, b = tank width, h_l = wave height at the endwall on the left side and h_r = wave height at the endwall on the opposite or right side. Eq. (2) is based on the assumption that the hydrostatic pressure force is dominant by neglecting both the inertial force due to the vertical acceleration of the liquid at the endwalls and the frictional force along the tank bottom. In this study, the base shear force of the TLD is numerically simulated as the hydrostatic pressure force by (2), in which the characterization of the wave height is based upon the shallow-water wave theory.

The shallow-water wave theory is based on the depth-averaged equations of mass and momentum conservation. The derivation of these equations involves the assumptions that water is an incompressible and inviscid fluid; that the water depth is infinitesimally small in comparison with the charac-

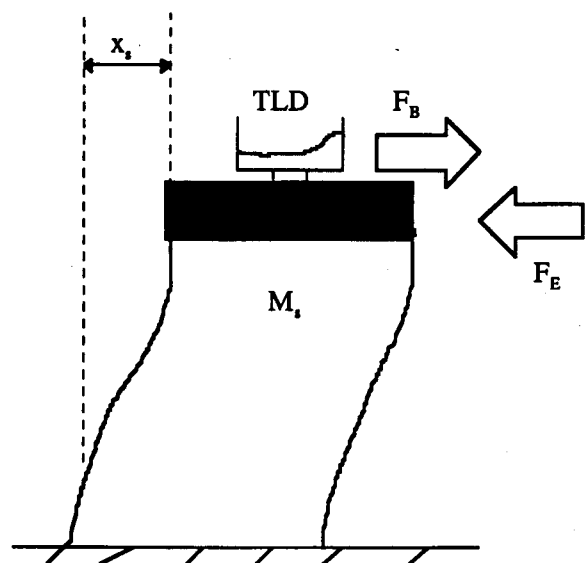


FIG. 1. Schematic of Tuned Liquid Damper Attached to Single-Degree-of-Freedom Structural System

¹Prof., Civ. Engr., Univ. of Washington, Seattle, WA 98195.

²Grad. Res. Asst., Univ. of Washington, Seattle, WA.

³Prof., Civ. Engr., Univ. of Washington, Seattle, WA.

⁴Grad. Res. Asst., Univ. of Washington, Seattle, WA.

Note. Associate Editor: P. K. Banerjee. Discussion open until September 1, 1998. To extend the closing date one month, a written request must be filed with the ASCE Manager of Journals. The manuscript for this paper was submitted for review and possible publication on September 12, 1996. This paper is part of the *Journal of Engineering Mechanics*, Vol. 124, No. 4, April, 1998. ©ASCE, ISSN 0733-9399/98/0004-0405-0413/\$4.00 + \$.50 per page. Paper No. 14081.

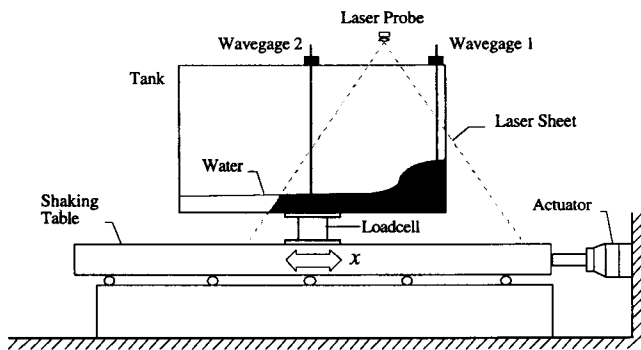


FIG. 3. Shaking Table Experimental Set-Up

where L = length of the tanks; and h_0 = water depth as illustrated in Fig. 2.

2. Excitation frequency ratio β

$$\beta = \frac{f_e}{f_w} \quad (6)$$

where f_e = frequency of the sinusoidal excitation.

3. Nondimensional water surface elevation η'

$$\eta' = \frac{\eta}{h_0} \quad (7)$$

where η = departure of the water surface from the undisturbed water surface depth, h_0 .

4. Nondimensional base shear force F'_w

$$F'_w = \frac{F_w}{m_w \omega^2 A} \quad (8)$$

where F_w = reaction force of the tank created by sloshing motions induced by the shaking table movement; m_w = mass of the water in the tank; ω = excitation angular frequency of the shaking table; A = shaking table excitation amplitude; and the product $m_w \omega^2 A$ = maximum inertia force of the water mass treated as a solid mass. In this analysis, the measured base shear force was obtained by subtracting the inertia force of the mass of the tank from the total force measured by the load cell to identify the force due to sloshing motion only.

5. Nondimensional phase angle ϕ' . The phase angle ϕ in radians between the shaking table motion and the base shear force has been expressed in units of π , as follows:

$$\phi' = \frac{\phi}{\pi} \quad (9)$$

6. Nondimensional energy dissipation per cycle E'_d

$$E'_d = \frac{E_d}{\frac{1}{2} m_w (\omega A)^2} \quad (10)$$

where the numerator is the energy dissipation per cycle is defined by

$$E_d = \int_{\tau_i} F_{wx} dx \quad (11)$$

where dx refers to integration over the shaking table displacement per cycle; and the denominator of (10) = the maximum kinetic energy of the water mass treated as a solid mass.

In addition to the wave-gauge and load-cell measurements, the spatial water-surface profiles were captured by video with the aid of a laser-light sheet. A typical image of the water-surface with wave breaking is shown in Fig. 4.



FIG. 4. Digitized Wave Profile Image from Shaking Table Test for Rectangular Tank of Length $L = 590$ mm

Time History Analysis

Examples of the typical data recorded under sinusoidal excitation for the rectangular tank of length $L = 590$ mm, water depth $h_0 = 30$ mm, and amplitude $A = 20$ mm at the base excitation frequency ratios β of 0.7, 1.0, 1.2 and 1.4, respectively, are given in Figs. 5(a-d). Figs. 5(a) and (b) contain plots of the temporal variations of the nondimensional water surface profiles near the end wall η'_1 and at the middle of the tank η'_2 , respectively. In Fig. 5(c), F_{wx} is the base shear force measured in the longitudinal or x-direction; the data have been filtered by a 5 Hz low-pass filter to eliminate system noise. In Fig. 5(d), F_{wy} is the base shear force measured in the transverse or y-direction. At the excitation frequency ratio of 0.7, small and smooth waves develop, as shown in Fig. 5(a). The water surface remains constant at the node of the standing wave at the middle of the tank, as shown in Fig. 5(b) with $\beta = 0.7$. This smooth back-and-forth wave formation with the node at the middle of the tank and the anti-nodes at the end walls is typical of the lowest mode of the standing wave that can be predicted with the linearized water-wave theory. At higher frequency ratios of unity and 1.2, strong waves develop and the saw-tooth wave formation, as shown in Figs. 5(a) and (b) with $\beta = 1$, represents wave breaking. The wave height at the end wall [Fig. 5(a)] is twice the height at the middle of the tank [Fig. 5(b)], which is consistent with the prediction by (3) and (4). The previously shown digitized image of Fig. 4 corresponds to the wave gauge data of the tank shown in Fig. 5(a) for excitation frequency ratio $\beta = 1.18$. Note that the wave motion dramatically decreases at $\beta = 1.4$.

Fig. 6 presents the time history responses for the water surface elevations at the end wall for the case of the tank with length $L = 590$ mm and water depth $h_0 = 30$ mm at various excitation frequencies for the excitation amplitudes $A = 10$, 20, and 40 mm, respectively. The excitation frequencies for which the time histories are shown in Fig. 6 were selected on the basis of the tank behavior under each excitation. Wave breaking over a wide range of frequencies is apparent by the strongly skewed wave profiles. It is noted that the largest wave motion in each case occurs at a frequency ratio higher than unity. In each case, this frequency ratio is different; the significance of this behavior is more fully explored in the frequency analysis section. Another observation is the characteristics of peaked crests and flattened troughs in the wave profile at the higher frequency ratios. This behavior clearly indicates a fairly complex wave pattern associated with strongly nonlinear characteristics.

Fig. 7 shows the corresponding base shear force due to sloshing motion. The base shear mirrors the wave motion results of Fig. 6. The largest forces are developed at frequency ratios higher than unity. Because the duration of these peaks is shorter, the influence of the force in mitigating structural motion is not clear; hence, an energy dissipation analysis is necessary. For the same cases, Fig. 8 contains plots of the base shear force versus the shaking table displacement for the three

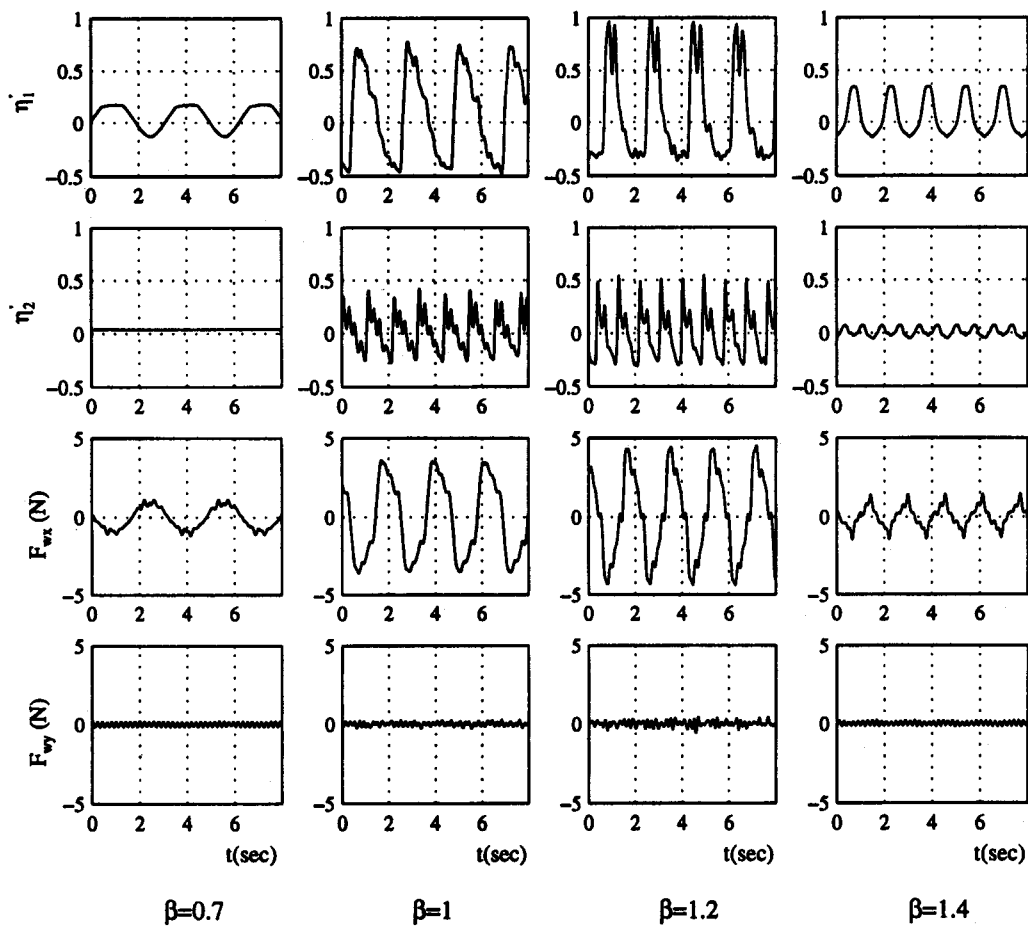


FIG. 5. Sample Time Histories of Water Sloshing Motion for Case of Tank with Length $L = 590$ mm, Water Depth $h_0 = 30$ mm and Amplitude of Excitation $A = 20$ mm

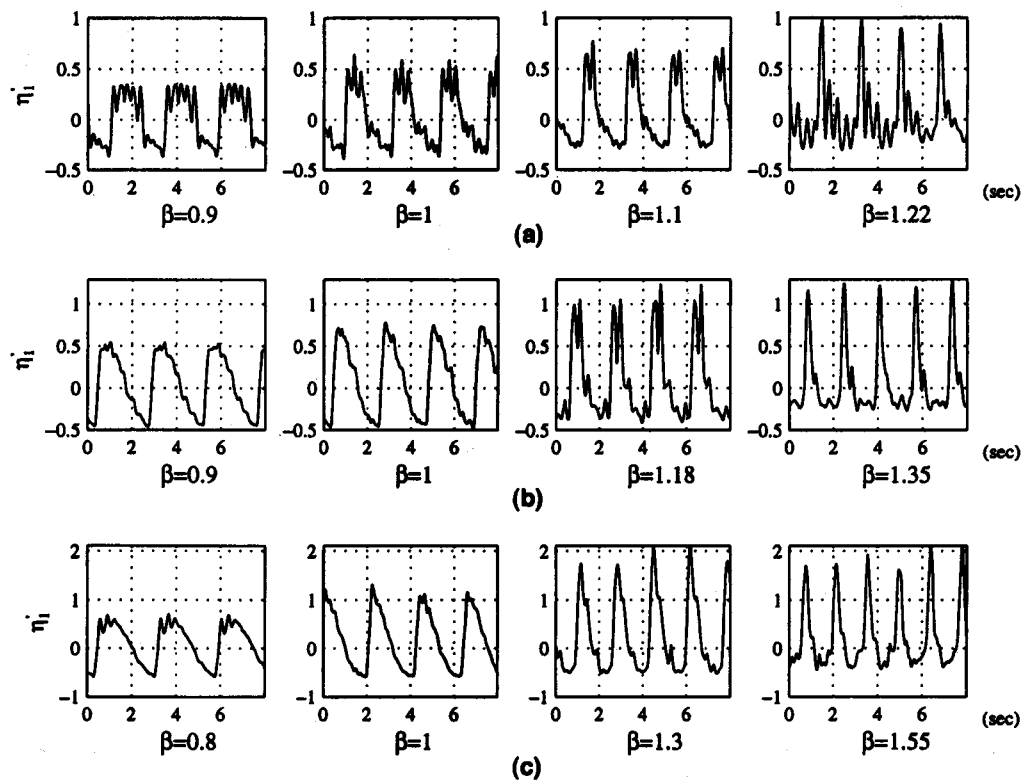


FIG. 6. Sample Time Histories of Nondimensional Endwall Wave Profiles for Tanks with Length $L = 590$ mm, and Water Depth $h_0 = 30$ mm: (a) Amplitude $A = 10$ mm; (b) $A = 20$ mm; (c) $A = 40$ mm

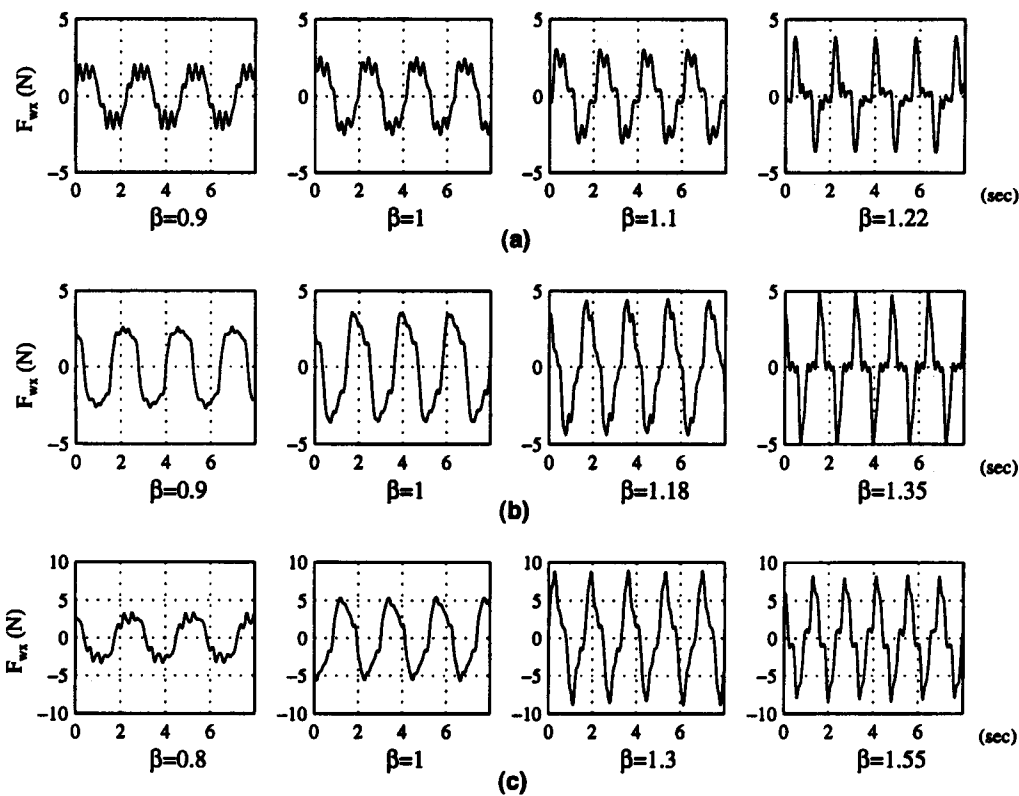


FIG. 7. Sample Time Histories of Measured Base Shear Force in x -Direction for Same Conditions as Fig. 6: (a) $A = 10$ mm; (b) $A = 20$ mm; (c) $A = 40$ mm

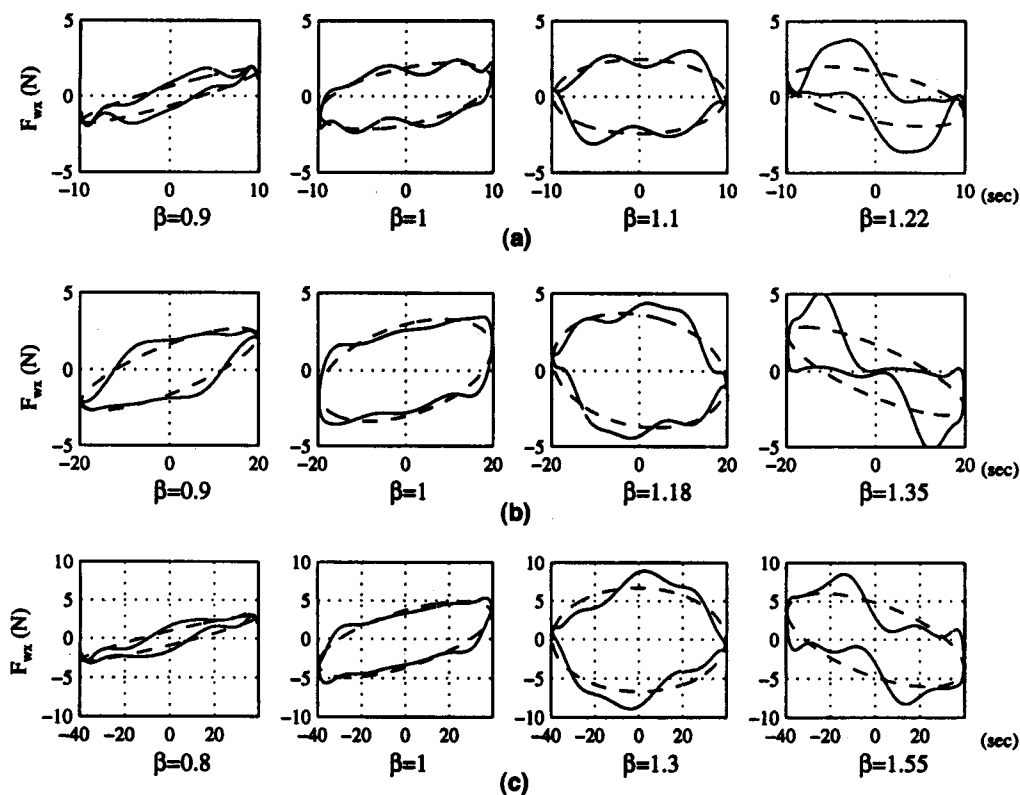


FIG. 8. Energy Dissipation Curves of Sloshing Force F_{wx} [N] versus Shaking Table Displacement x [mm] for Same Conditions as Fig. 7: (a) $A = 10$ mm; (b) $A = 20$ mm; (c) $A = 40$ mm

amplitudes of excitation $A = 10, 20$, and 40 mm, respectively, and at excitation frequency ratios, β , below, at, and above unity. The dashed lines indicate the base shear forces, including only the fundamental mode of water sloshing. The solid lines indicate the base shear forces, including higher modes. The effects of the higher modes of water sloshing motions on

the time history base shear forces can be determined by comparing these two curves. The higher modes change the time history of the magnitude of the base shear forces. However, the areas inside the loops do not change significantly. For example, for the tank whose results are shown in Fig. 8(b), of length $L = 590$ mm, $h_0 = 30$ mm, and $A = 20$ mm, the differ-

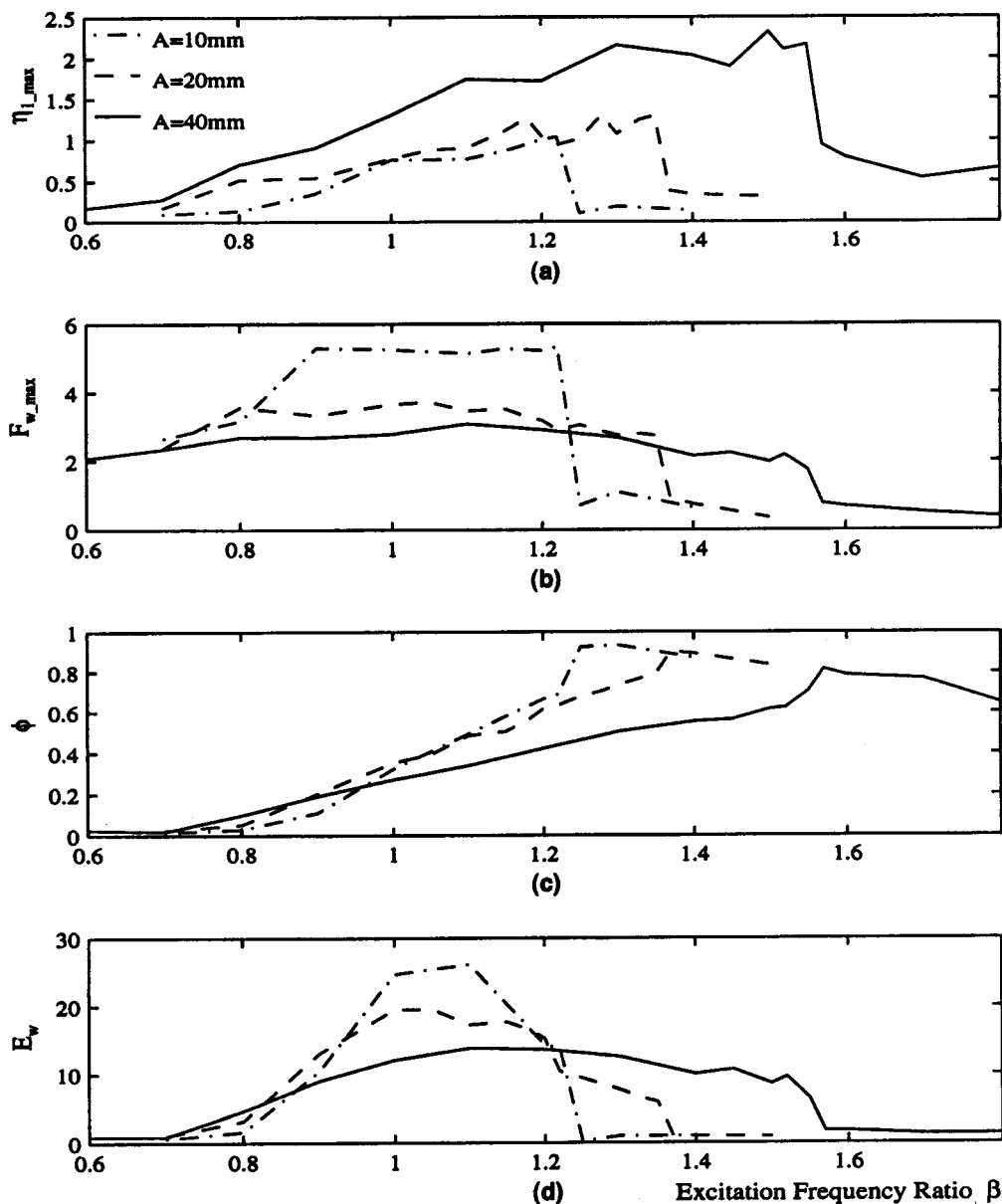


FIG. 9. Sample Frequency Response Curves for Shaking Table Tests of Tank with Length $L = 590$ mm, $h_0 = 30$ mm, and Excitation Amplitudes of $A = 10, 20$, and 40 mm: (a) Maximum Wave Height near End Wall; (b) Maximum Base Shear Force; (c) Phase Angle between F_w and x ; (d) Energy Dissipation per Cycle

ence in the areas computed for the energy dissipation using the two representations is about 2%.

The performance of TLDs can be assessed through calculating the area enclosed by the contours shown in Fig. 8, as this represents the energy dissipation during a cycle of motion. To ensure large dissipation at steady state, the ideal phase angle should be $\pi/2$, which yields a contour symmetrical about the F_{wx} axis, just as those at $\beta = 1.1$ in Fig. 8(a), at $\beta = 1.18$ in Fig. 8(b), and at $\beta = 1.3$ in Fig. 8(c). This condition is represented by a contour in which the area is at a maximum. When the contour in Fig. 8 becomes "flattened" in the diagram [see the contours at $\beta = 0.9$ in Fig. 8(a) and at $\beta = 0.8$ in Fig. 8(c)], it represents the situation when damper loses its effectiveness. Furthermore, when the contour trajectory becomes clockwise, the damper behaves adversely, i.e., negative damping will occur. It must be emphasized that the adverse dissipation never occurred throughout our experiments, which covered wide excitation frequency and tank ranges. The results shown in Fig. 8 suggest that the damper performance can be predicted approximately by analyzing the fundamental mode

of water sloshing alone without examining the higher-mode effects even for the cases with strong excitation.

Frequency Analysis

In addition to the time history analyses, the same parameters of wave height and base shear were plotted versus the excitation frequency ratio. For the tank of length $L = 590$ mm with water depth of $h_0 = 30$ mm, the effect of the base excitation amplitude on the wave motion was examined for the excitation amplitudes $A = 10, 20$, and 40 mm. The results are shown in Fig. 9 for maximum wave height, maximum base shear force, phase angle between the fundamental mode of the base shear force F_{wx} and the shaking table displacement x , and the energy dissipation per cycle. All quantities are in nondimensional form as defined in (6)–(10). It can be seen that the wave height increases as the excitation frequency approaches the natural frequency of the TLD; however, the peak occurs at an excitation frequency much higher than the tank natural frequency, which clearly demonstrates the nonlinear behavior of

the fluid in the tank. After a gradual, fairly smooth build-up to a peak value, there is a dramatic drop in value. This phenomenon has been remarked upon by previous researchers (e.g., Lepelletier and Raichlen 1988; Sun et al. 1991); it is called the "jump" phenomenon, and the frequency at which it occurs is called the "jump frequency," f_{jump} . The existence of the jump frequency at frequency ratios $\beta > 1.0$ indicates that the water sloshing motion displays a "hardening" or "stiffening" spring-type nonlinearity. These results are qualitatively consistent with the data provided by Fujino et al. (1992) for similar experiments but with much smaller excitation. The maximum excitation amplitude to tank length ratio in their investigation was $A/L = 0.0169$, whereas the present experiments included the case with $A/L = 0.0678$.

The curves in the plot of the phase angle shown in Fig. 9(c) exhibit gentle slopes. Also note that the nondimensionalized phase angle ϕ' never exceeds unity (or the actual phase angle ϕ is always between 0 and π). This means that, for the frequency range we tested, the TLD never behaved adversely (no negative damping occurred). The corresponding energy dissipation plot for the three excitation amplitudes shows that as amplitude increases, energy dissipation over a broader range of frequencies occurs. The dissipation over a broad range in this manner illustrates that the tank is a robust energy-dissipating system.

From Fig. 9(a), it can be seen that as the excitation amplitude increases, the value of the jump frequency ratio and the response increases. This increase indicates that the nonlinearity of the water sloshing motion becomes stronger as the excitation amplitude increases. This hardening spring behavior can be explained physically by the fact that the wave propagation speed in shallow water depends on the wave amplitude. Based on the shallow-water wave theory, the propagation speed, S , for a nonbreaking wave is $\sqrt{g(h_0 + \eta)}$. For the quasi-steady response of the sloshing motion to the forcing equation, the excitation frequency, f , and the wave propagation speed, S , must be related by

$$f = \frac{S}{2L} \quad (12)$$

where L = tank length. Eq. (12) indicates that as the excitation frequency increases, the wave must propagate faster. Consequently, the wave amplitude must increase, and ultimately, greater response results. A similar observation can be made in the case of broken waves such as that shown in Fig. 4. Considering the wave breaking to be a bore propagating on a quiescent water of depth h_t , the propagation speed, S , of the breaking wave can be evaluated as

$$S = \sqrt{\frac{g}{2} \frac{h_{II}}{h_t} (h_t + h_{II})} \quad (13)$$

based on the shallow-water wave theory (3) and (4). In (13), h_{II} is the total water depth immediately behind the wave front. Approximating the average propagation speed associated with the tank sloshing by the wave front speed at the middle of the tank, the relationship between the wave height ($\Delta h = h_{II} - h_t$) and the forcing frequency estimated by (12) was plotted in Fig. 10. This figure shows that a TLD adjusts to an increased wave height when the excitation frequency increases and in so doing enhances the damping performance.

The relationship between the jump frequency and nondimensional excitation amplitude is shown in Fig. 11. This plot includes previous results of Sun et al. (1992) for small amplitude motion. Although the damper is assumed to no longer be effective at excitation frequencies greater than the jump frequency, the results in Fig. 11 clearly indicate that, when the excitation amplitude increases, the frequency range of damper effectiveness widens. Fig. 11 further illustrates that when the

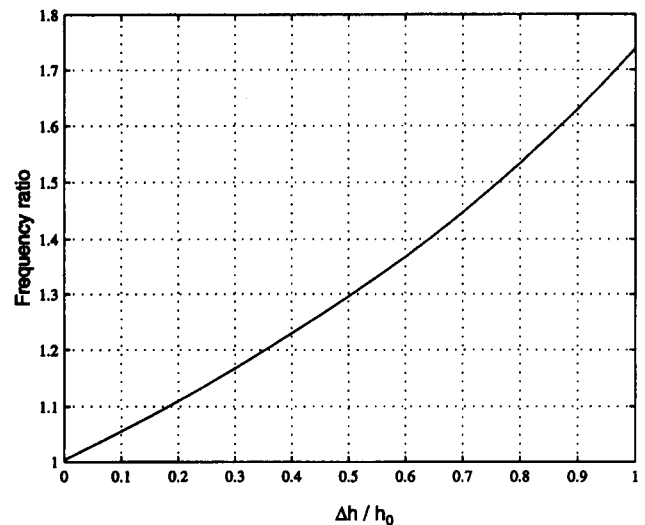


FIG. 10. Relationship between Water Frequency Ratio of f to f_n , where f is Defined by Eq. (12) and f_n is Defined by Eq. (5), and Nondimensional Water Wave Height $\Delta h/h_0$, where Δh is Defined in Eq. (13)

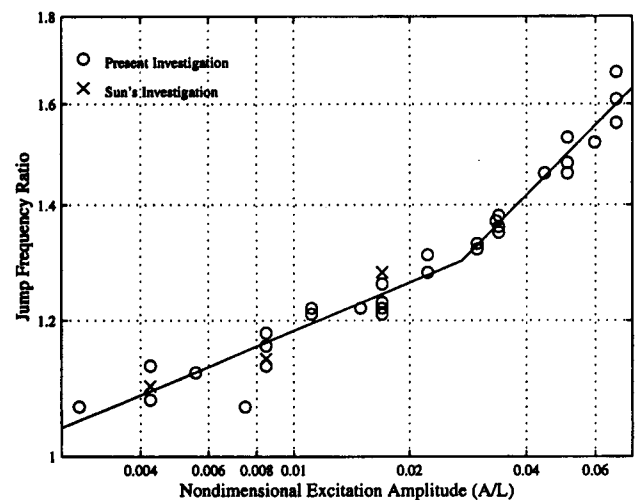


FIG. 11. Relationship between Jump Frequency Ratio and Nondimensional Excitation Amplitude Based on Experimental Results of Sun et al. (1991) and Present Investigation

excitation amplitude goes beyond the value of approximately $A/L > 0.025$, the slope of the curve increases. This change implies that the rate at which the range of frequencies for which the damper is effective increases. Therefore, the tuned liquid damper performs in a wider frequency range under strong excitation. This behavior also suggests that the nonlinear behavior is responsible for the improved performance and robustness of the rectangular TLD.

NUMERICAL ANALYSIS

A series of numerical simulations of the tank sloshing were undertaken using the random choice method to solve the shallow-water wave equations, (3) and (4). The results presented here correspond to the simulation for the $L = 590$ mm tank whose experimental behavior was shown in Figs. 5 and 6. The length of the tank was meshed with 400 grid points. The hydrodynamic force was computed by the hydrostatic pressure forces described in (2).

Fig. 12(a) shows the time history of water-surface profile for the conditions of a tank with length $L = 590$ mm, water depth $h_0 = 30$ mm, and an excitation amplitude of $A = 20$ mm. The profile in Fig. 12 is at 1.7 cm from the end wall, where

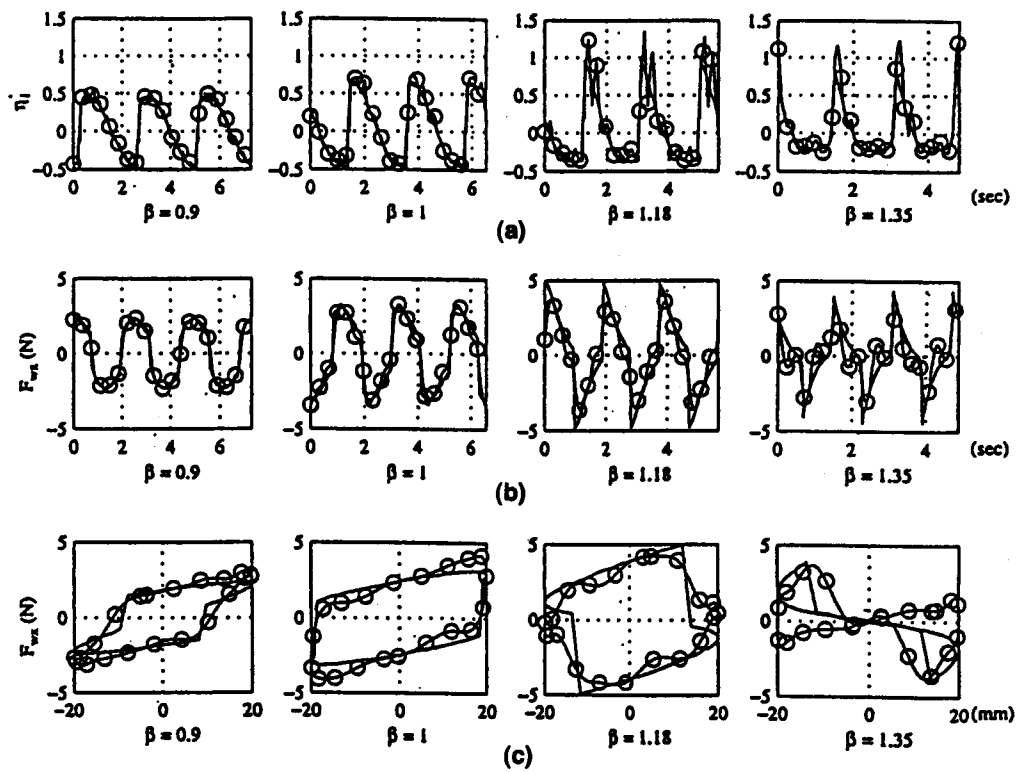


FIG. 12. Comparison of Numerical Simulation Using Random Choice Method (—o—) and Measured Data (—) for Rectangular Tank of Length $L = 590$ mm, $h_0 = 30$ mm, and Excitation Amplitude $A = 20$ mm, for Various Excitation Frequency Ratios: (a) Wave Height at End Wall; (b) Base Shear Force; (c) Energy Dissipation

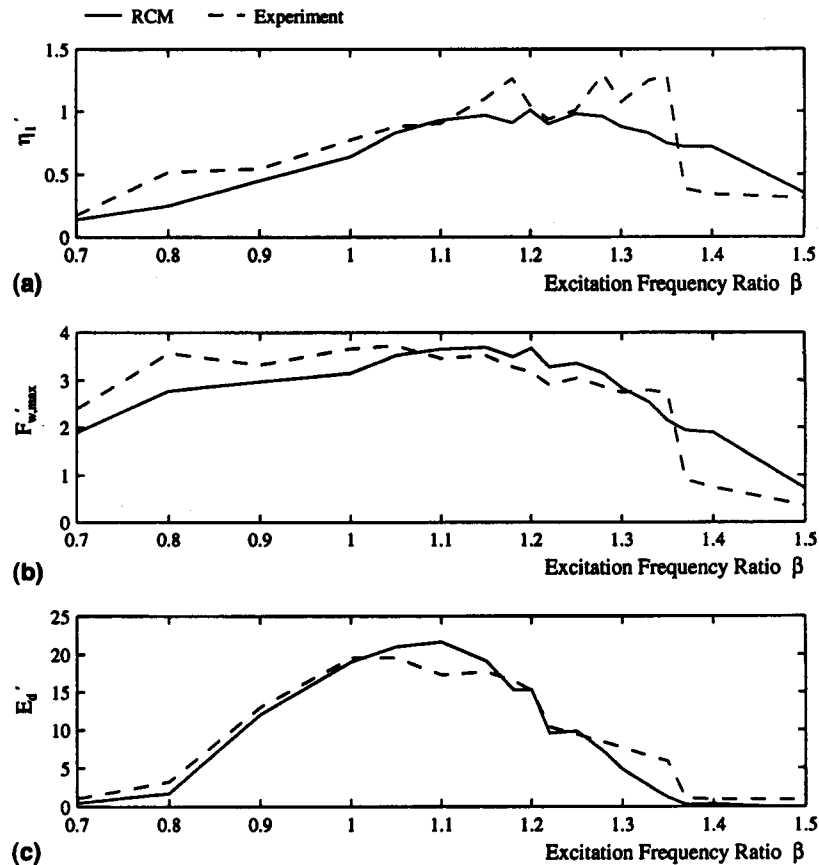


FIG. 13. Frequency Response Comparisons Using Shaking Table Data and Random Choice Method for Rectangular Tank of Length $L = 590$ mm, $h_0 = 30$ mm, and Excitation Amplitude $A = 20$ mm: (a) Maximum Wave Height near End Wall; (b) Maximum Base Shear Force; (c) Energy Dissipation per Cycle

one of the wave gauges was placed in the shaking table tests. The numerical predictions are compared with the experimental data. It is emphasized that there is absolutely no "tweaking" parameter involved in the numerical model. The random-choice-method simulation accurately predicts the period and amplitude of the waves, even for the cases where large wave breaking occurs. The greatest discrepancy between the data and the simulation is in capturing the short trailing waves behind the leading wave. Because the random choice method solves the fully nonlinear but non-dispersive shallow-water wave equations, (3) and (4), it is not capable of modeling these dispersive waves. The wave heights generated by the numerical model behind the leading wave are about the average height of the trailing waves. The model predicts a sharper rise in the wave heights when the leading wave hits the end wall than that observed in the shaking table tests. This is due to the fact that the real bore front has a finite width but the simulated bore front extends only between two grid points, i.e., the discontinuity.

The sloshing forces were numerically simulated using the hydrostatic pressure assumption by (2). The calculated forces are compared to the load-cell data in Fig. 12(b). The model predicts quite accurately the force when wave breaking is not the dominant feature of the flow (e.g., for $\beta = 0.9$ and 1.0). The predictions for the larger amplitudes are not as accurate behind the leading wave where the trailing waves influence the force. This discrepancy is expected in light of the previous discussion about the limitation of the shallow-water wave theory. The numerical model appears to consistently overpredict the forces. This overprediction may result from excluding the effect of inertial forces created by the vertical acceleration along the end wall.

The computed base shear force was plotted against the shaking table displacement in Fig. 12(c), with the measured data of Fig. 8(b) also shown for comparison. The representation by the random choice method is good for the lower frequency ratios. Although the agreement overall is fairly good, the model is not accurate near the jump region ($\beta = 1.35$).

Fig. 13 contains the frequency analysis comparing the simulations and the measured data. The simulated results are in good agreement with the experimental results; however, the jump phenomenon is not captured, as seen in Fig. 13(a) and (b). The numerical scheme predicts a much gentler, smoother transition over the frequency range for the wave profile and maximum base shear force. On the other hand, the energy dissipation curve compares very well for the entire frequency range, with slight discrepancies near the excitation ratio of unity and in the jump region. This result suggests that the random choice method has potential for capturing the energy dissipation when evaluated in this manner rather than strictly through the base shear force-displacement plots of Fig. 12(c). While the model does not simulate exactly the wave motion over the entire frequency range, it does provide an excellent approximation of the TLD performance through the energy dissipation over the entire range. This particular result is encouraging, given that the design process may ultimately be formulated upon the maximum performance as defined by the estimated energy dissipation.

CONCLUSIONS

Experimental investigation and numerical modeling of liquid behavior in TLDs have provided insight into the behavior of these devices in controlling structural vibration under small and large amplitude excitation. Not only were previous limited measurements expanded to large amplitude excitation more representative of earthquake motion, the analysis of these large

amplitude results was considerably enhanced by evaluating the results through the shallow-water wave theory. The results suggest that nonlinear tuning of the tanks is appropriate; that the tanks are robust in dissipating energy over a wide frequency range, particularly for large amplitude excitation; and that caution for design of tanks for excitation for high frequency ratios should be exercised due to the jump phenomenon. Because of its robustness and hardening spring behavior, the design damper frequency (if it is evaluated by the linearized wave theory) must be tuned at the value lower than that of the structural response frequency.

ACKNOWLEDGMENTS

We would like to thank Dr. Sami Masri for arranging the use of the shaking table facility at the University of Southern California. Dr. T. Wakahara assisted our laboratory experiments. The support of the U.S. National Science Foundation (Grant No. CMS-9301577) for this project is gratefully acknowledged.

APPENDIX. REFERENCES

- Chorin, A. J., and Marsden, J. E. (1979). *A Mathematical Introduction to Fluid Mechanics*. Springer-Verlag, Inc., New York, N.Y.
- Fediw, A. A., Breukelman, B., Morris, D. P., and Isyumov, N. (1993). "Effectiveness of a tuned sloshing water damper to reduce the wind-induced response of tall buildings." *Proc., 7th U.S. National Conference on Wind Engineering*, Vol. 1, Univ. of California, Los Angeles, Calif., 233–242.
- Fujii, K., Tamura, Y., Sato, T., and Wakahara, T. (1990). "Wind-induced vibration of tower and practical applications of tuned sloshing damper." *J. Wind. Eng. and Ind. Aerodyn.*, 33, 263–272.
- Fujino, Y., Sun, L., Pacheco, B. M., and Chaiseri, P. (1992). "Tuned liquid damper for suppressing horizontal motion of structures." *J. Engrg. Mech.*, ASCE, 118(10), 2017–2030.
- Gardarsson, S., and Yeh, H. (1994). "Numerical simulations of bores using the random-choice method." *Proc., 3rd UJNR Tsunami Workshop*, Public Works Research Council, Ministry of Construction, Tsukuba, Japan, 13–23.
- Glimm, J. (1965). "Solution in the large for nonlinear hyperbolic systems of equations." *Commun. Pure and Appl. Math.*, 18, 697–715.
- Holt, M. (1984). *Numerical methods in fluid dynamics*. Springer-Verlag KG, Berlin, Germany.
- Kareem, A., and Sun, W.-J. (1987). "Stochastic response of structures with fluid-containing appendages." *J. Sound and Vibration*, 119(3), 389–408.
- Koh, C. S., Mahatma, S., and Wang, C. M. (1994). "Theoretical and experimental studies on rectangular dampers under arbitrary excitations." *Earthquake Engrg. and Struct. Dynamics*, 23, 17–31.
- Lamb, H. (1932). *Hydrodynamics*. Cambridge University Press, London, England.
- Lax, P. D., and Wendroff, B. (1964). "Difference schemes for hyperbolic equations with high order of accuracy." *Commun. on Pure and Appl. Math.*, 17, 381–398.
- Lepelletier, T. G., and Raichlen, F. (1988). "Nonlinear oscillations in rectangular tanks." *J. Engrg. Mech.*, ASCE, 114(1), 1–23.
- Sun, L. M., Fujino, Y., Pacheco, B. M., and Chaiseri, P. (1991). "Modeling tuned liquid dampers." *Proc., 8th International Conference on Wind Engineering*, International Association for Wind Engineering, London, Ontario, Canada, 1883–1894.
- Sun, L. (1991). "Semi-analytical modeling of tuned liquid damper (TLD) with emphasis on damping of liquid sloshing." PhD thesis, University of Tokyo, Tokyo, Japan.
- Tamura, Y., Fujii, K., Sato, T., Wakahara, T., and Kosugi, M. (1988). "Wind-induced vibration of tall towers and practical applications of tuned sloshing dampers." *Proc., Symposium on Serviceability of Buildings*, University of Ottawa, Ottawa, Canada, 1.
- Wakahara, T., Ohyama, T., and Fujii, K. (1992). "Suppression of wind-induced vibration of a tall building using the tuned liquid damper." *J. Wind Eng. and Ind. Aerodyn.*, 41–44, 1895–1906.
- Wakahara, T. (1993). "Wind-induced response of TLD-structure coupled system considering nonlinearity of liquid motion." *Shimizu Tech. Res. Bull.*, 12, 41–52.
- Wakahara, T., Fujino, Y., and Nomura, T. (1996). "Nonlinear sloshing analysis of a circular tuned liquid damper using the Boussinesq equation." *Proc., JSCE*, Tokyo, Japan, 549, 125–140.